PHYSICAL REVIEW B VOLUME 19, NUMBER 8 15 APRIL 1979

Lattice dynamics of a 15-layer unrelaxed MgO (001) slab: Breathing-shell model

R. N. Barnett and Ronald Bass
Department of Physics and Astronomy, University of Kansas, Lawrence, Kansas 66045
(Received 13 December 1978)

The lattice dynamics of a 15-layer unrelaxed MgO (001) slab is studied using a breathing-shell model and the results are compared to previous non-breathing-shell model and experimental results. An efficient method of integrating over the surface Brillouin zone, involving one-dimensional integrals along several "special directions" is outlined. In general the results are similar to the non-breathing-shell model results. However, a new surface mode is found at the lower edge of the LO bulk band, and the surface-excess-distribution function shows peaks not found in the non-breathing-shell model result.

I. INTRODUCTION

Recently there has been a considerable amount of interest in theoretical studies of surface modes of vibration in ionic crystals. The most successful approach has been that of slab lattice dynamics in which the normal modes are obtained for a slab-shaped crystal of finite thickness. Chen *et al.*[1] have recently reported the results of a comprehensive study of the unrelaxed (001) surfaces of seven ionic crystals having the rocksalt structure. The crystals studied were six alkali halides and MgO. The normal- or non-deformable-shell model was used. The purpose of the present paper is to report the effect of incorporating a breathing mode on the normal modes of vibration of an unrelaxed MgO (001) slab and to form a basis for future calculations including surface relaxation.

The breathing-shell model has been shown by Sangster *et al.*[2] to be superior to the normal-shell model in describing the bulk lattice dynamics of MgO, particularly the high-frequency modes where the effect of surface relaxation is expected to be most pronounced. In addition, in the breathing-shell model, the forces may be taken to be central even though the elastic constants do not satisfy the Cauchy relations $C_{12}=C_{44}$, provided that $C_{12}>C_{44}$, as is the case for MgO.[3] We have previously reported the results of a self-consistent calculation of the relaxation of an MgO slab due to the free (001) surfaces[4] and have found that the breathing mode produced significant contributions to the surface energy and the relaxed configuration. The present paper is restricted to the unrelaxed case and a future publication will deal with the relaxed surfaces.

The paper is organized as follows. In Sec. II we briefly describe the model and how the breathing mode is included, and discuss the method used to obtain the frequency distribution functions. The results for a 15-layer MgO (001) slab are reported in Sec. III, we compare our results with the normal-shell-model results of Chen *et al.*[1] and with the experimental surface-excess-distribution function of Rieder.[5]

II. MODEL AND CALCULATIONS

The breathing-shell model used in the slab lattice-dynamics calculations reported here is equivalent in the limit of an infinite number of layers to model E of Ref. 2; the definitions and numerical values of the parameters are given there. In this model each ion consists of a positively charged core surrounded by a negatively charged shell. The shell may be displaced with respect to its core, taking into account the polarizability of the ions. The breathing mode consists of an isotropic deformation, or a change in radius, of the shell. Short-range interactions between ions are assumed to take place only between the shells so that a decrease in radius of a shell will have the same effect on the non-Coulomb interaction with a neighboring ion as a displacement away from that ion.

We define $\vec{u}(\vec{l}\kappa)$, $\vec{w}(\vec{l}\kappa 0)$, and $v(\vec{l}\kappa)$ to be the core displacement, the shell displacement with respect to its core, and isotropic shell distortion of the κth ion at lattice site $\vec{l}$. Since translational invariance still applies in directions parallel to the surfaces these variables will be two-dimensional Block functions $\vec{u}(l_3\kappa;\vec{q})$, $\vec{w}(l_3\kappa;\vec{q})$ and $v(l_3\kappa;\vec{q})$, where l_3 is the component of $\vec{l}$ normal to the surfaces and $\vec{q}$ is the two-dimensional wave vector parallel to the surfaces. The equations of motions may be expressed as follows:

$$m_\kappa\omega^2\vec{u}(l_3\kappa;\bar{q}) = \sum_{l_3'\kappa'} [z_\kappa z_{\kappa'}\vec{C}(l_3\kappa, l_3'\kappa';\bar{q})\cdot\vec{u}(l_3'\kappa';\bar{q}) + z_\kappa y_{\kappa'}\vec{C}(l_3\kappa, l_3'\kappa';\bar{q})\cdot\vec{w}(l_3'\kappa';\bar{q}) + \vec{R}(l_3\kappa, l_3'\kappa';\bar{q})\cdot\vec{u}(l_3'\kappa';\bar{q}) + \vec{R}(l_3\kappa, l_3'\kappa';\bar{q})\cdot\vec{w}(l_3'\kappa';\bar{q}) + \vec{Q}(l_3\kappa, l_3'\kappa';\bar{q})v(l_3'\kappa';\bar{q})],$$

$$0 = \sum_{l_3'\kappa'} [y_\kappa z_{\kappa'}\vec{C}(l_3\kappa, l_3'\kappa';\bar{q})\cdot\vec{u}(l_3'\kappa';\bar{q}) + y_\kappa y_{\kappa'}\vec{C}(l_3\kappa, l_3'\kappa';\bar{q})\cdot\vec{w}(l_3'\kappa';\bar{q}) + \vec{R}(l_3\kappa, l_3', \kappa';\bar{q})\cdot\vec{u}(l_3'\kappa';\bar{q}) + \vec{R}(l_3\kappa, l_3'\kappa';\bar{q})\cdot\vec{w}(l_3'\kappa';\bar{q}) + \vec{Q}(l_3\kappa, l_3'\kappa';\bar{q})v(l_3'\kappa';\bar{q})] + y_\kappa(z_\kappa - y_\kappa)\vec{C}(l_3\kappa, l_3\kappa;\bar{0})\cdot\vec{w}(l_3\kappa;\bar{q}) + K_\kappa\vec{w}(l_3\kappa;\bar{q}),$$

$$0 = \sum_{l_3'\kappa'} [\vec{Q}^*(l_3'\kappa', l_3\kappa;\bar{q})\cdot\vec{u}(l_3'\kappa';\bar{q}) + \vec{Q}^*(l_3'\kappa', l_3\kappa;\bar{q})\cdot\vec{w}(l_3'\kappa';\bar{q}) + H(l_3\kappa, l_3'\kappa';\bar{q})v(l_3'\kappa';\bar{q})] + G_\kappa v(l_3\kappa;\bar{q}),$$

where m_κ is the mass of the κth ion, z_κ is the total charge, and y_κ is the shell charge of the κth ion, and K_κ and G_κ are spring constants associated with shell displacement and isotropic distortion, respectively. The matrix elements $C_{\alpha\beta}(l_3\kappa, l_3'\kappa';\bar{q})$ and $R_{\alpha\beta}(l_3\kappa, l_3'\kappa';\bar{q})$, where $\alpha,\beta = 1,2,3$ describe, respectively, the Coulomb and short-range interactions and are identical, except for a factor of $1/\sqrt{m_\kappa m_{\kappa'}}$, to those given in Appendix C of Ref. 1. $\vec{C}(l_3\kappa, l_3'\kappa';\bar{0})$ is diagonal and is equivalent to $\Phi_{\alpha\alpha}(l_3\kappa, l_3\kappa;0)$ of Ref. 1. The elements $Q_\alpha(l_3\kappa, l_3'\kappa';\bar{q})$ and $H(l_3\kappa, l_3'\kappa';\bar{q})$ describe, respectively, the core or shell-displacement–shell-breathing and the shell-breathing–shell-breathing interactions and are given in the Appendix of this paper. The sums over l_3' are understood to include only the layers in the slab.

The polarization and shell breathing of the magnesium ion are assumed to be negligable with respect to the oxygen ion. This is equivalent to letting K_2/K_1 and G_2/G_1 become zero where $\kappa = 1$ for Mg and $\kappa = 2$ for O. In this case $w(l_3 1;\bar{q})$ and $v(l_3 1;\bar{q})$ will be identically zero and may be omitted from the equations.

The shell displacement and breathing can now be eliminated to obtain the dynamical matrix for core displacements. We define U to be a column matrix of the core displacements, W and V to be column matrices of the shell displacement and breathing, and a column matrix $X = (W, V)^T$. The equations of motion may be expressed in matrix form:

$$\begin{bmatrix} D_{cc} & D_{cs} \\ D_{cs}^\dagger & D_{ss} \end{bmatrix}\begin{bmatrix} U \\ X \end{bmatrix} = \omega^2\begin{bmatrix} MU \\ 0 \end{bmatrix},$$

where D_{cc} is an Hermitian matrix containing all the core-core interactions, D_{ss} is an Hermitian matrix containing all the shell-shell interactions and D_{cs} is a nonsquare complex matrix containing the core-shell interactions. The determination of the individual elements from the equations of motion given earlier is straightforward and need not be shown here. M is the diagonal matrix of ionic masses.

Now if we define $M^{-1/2}\zeta(\bar{q}) = U(\bar{q})$, where $M^{-1/2}$ is a diagonal matrix of elements $1/\sqrt{m_\kappa}$, then the dynamical matrix is

$$D = M^{-1/2}(D_{cc} - D_{cs}D_{ss}^{-1}D_{cs}^\dagger)M^{-1/2}.$$

The eigenvalues and eigenvectors of the dynamical matrix are the squared frequencies $\omega^2(\bar{q}p)$ and the normal modes $\zeta(\bar{q}p)$, $p = 1, \ldots, 6N$, N is the number of layers.

The dynamical matrix D is a $6N \times 6N$ Hermitian matrix. Allen *et al.*[6] show that if the slab has either axial-inversion symmetry or a three-dimensional center of inversion the matrix may be reduced to a real symmetric matrix of the same size and that if both of these symmetries are present it may be block diagonalized into two real symmetric matrices of approximately equal sizes (equal sizes of N is an even number). For a 15-layer slab the two matrices are 46×46 and 44×44. The components of the eigenvectors of the larger matrix which are parallel to the surfaces are symmetric about the center plane of the slab and the components normal to the surfaces are antisymmetric about the center plane. These modes will be referred to as symmetric modes. The opposite is true of the components of the eigenvectors of the smaller matrix and these modes will be called antisymmetric.

In performing the integral over the Brillouin zone (BZ) we need the quantity $[\nabla_q\omega(\bar{q}p)]\cdot\hat{q}$, i.e., the derivative of ω with respect to $|\bar{q}|$ in the direction of $\bar{q}$. We can show that

$$\nabla_q\omega(\bar{q}p) = [1/2\omega(\bar{q}p)]\{\Gamma^{-1}(\bar{q})[\nabla_q D(\bar{q})]\Gamma(\bar{q})\}_{pp},$$

where Γ is a matrix made up of the eigenvectors of D such that

$$[\Gamma^{-1}(\bar{q})D(\bar{q})\Gamma(\bar{q})]_{pp'} = \delta_{pp'}\omega^2(\bar{q}p).$$

Thus the derivative of $\omega(\bar{q}p)$ in any direction $\hat{k}$ is

given by

$$[\nabla_q w(\bar{q}p)]\cdot\hat{k} = [1/2\omega(\bar{q}p)]\{\Gamma^{-1}(\bar{q})[\nabla_q D(\bar{q})\cdot\hat{k}]\Gamma(\bar{q})\}_{pp}.$$

This expression is useful in drawing the dispersion curves as well as in the BZ integration.

After some simple matrix manipulations we find that

$$\nabla D = M^{-1/2}\{(\nabla D_{cc}) - [(\nabla D_{cs})D_{ss}^{-1}D_{cs}^{\dagger}] - [(\nabla D_{cs})D_{ss}^{-1}D_{cs}^{\dagger}]^{\dagger} + [(D_{ss}^{-1}D_{cs}^{\dagger})^{\dagger}(\nabla D_{ss})(D_{ss}^{-1}D_{cs}^{\dagger})]\}M^{-1/2}.$$

The matrices (∇D_{ab}), where $a, b = c$ or s, are obtained by simply taking the gradient of the individual elements. This method is superior to both interpolation or extrapolation procedures since the time consuming process of diagonalizing the dynamical matrix need be done only once for each $\bar{q}$ and the problems arising from the close approach or crossing of dispersion curves are avoided.

The frequency distribution functions are defined as follows:

$$g_b(\omega) = \frac{1}{6}\,\frac{2r_0^3}{(2\pi)^3}\int_{BZ} d^3q \sum_{p=1}^{6} \delta(\omega - \omega(\bar{q}p))$$

for the bulk,

$$g_s(\omega) = \frac{1}{6N}\,\frac{2r_0^2}{(2\pi)^2}\int_{BZ} d^2q \sum_{p=1}^{6N} \delta(\omega - \omega(\bar{q}p))$$

for the slab, and

$$f(\omega) = \tfrac{1}{2}N[\,g_s(\omega) - g_b(\omega)]$$

is the surface excess distribution function, where r_0 is the nearest-neighbor distance. To perform the BZ integration for the bulk we have used the "special directions" method of A. Bansil[7] and an analogous two-dimensional method, Gauss-Chebyschev integration, for the slab. In these methods the distribution function is approximated by

$$g(\omega) = \frac{1}{N_d}\sum_{i=1}^{N_d} \tilde{g}(\omega, \hat{q}_i),$$

where N_d is the number of special directions specified by unit vectors $\hat{q}_i$, and

$$\tilde{g}_b(\omega, \hat{q}_i) = \frac{1}{6}\,\frac{2r_0^3}{(2\pi)^3}\int_0^{q_{\max}(\hat{q}_i)} q^2\, dq \sum_{p=1}^{6} \delta(\omega - \omega(\hat{q}_i, qp)),$$

$$\tilde{g}_s(\omega, \hat{q}_i) = \frac{1}{6N}\,\frac{2r_0^3}{(2\pi)^3}\int_0^{q_{\max}(\hat{q}_i)} q\, dq \sum_{p=1}^{6N} \delta(\omega - \omega(\hat{q}_i, qp)).$$

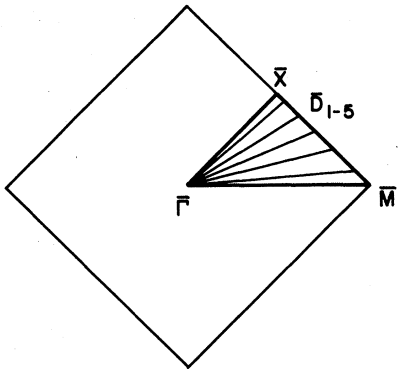

FIG. 1. Surface Brillouin zone (SBZ). The irreducible element is bounded by the high-symmetry lines $\bar{\Gamma}\bar{X}$, $\bar{X}\bar{M}$, and $\bar{M}\bar{\Gamma}$. The five "special directions," $\bar{\Gamma}\bar{D}_1$-$\bar{\Gamma}\bar{D}_5$ used in the SBZ integration are also shown, ΓD_1 being closest to $\bar{\Gamma}\bar{X}$.

The one-dimensional integrals involved in $\tilde{g}(\omega, \hat{q}_i)$ were obtained by evaluating $\omega(\hat{q}_i, qp)$ and $\nabla\omega(\hat{q}_i, qp)\cdot\hat{q}_i$ for 50 evenly spaced points along the special directions, then using $\nabla\omega\cdot\hat{q}_i$ to approximate ω between the evenly spaced points. For the bulk calculation we have used the 13 special directions given in footnote 7 of Ref. 7. In the two-dimensional slab case the special directions are given by the angle $\phi_i(N_d) = (2i-1)\pi/8N_d$ between $\hat{q}_i$ and the line $\bar{\Gamma}\bar{X}$ (see Fig. 1). For the slab calculation reported in Sec. III we have used $N_d = 5$.

To verify our calculations we have compared our results to the results of previous calculations. We reproduced the frequencies quoted for models B and E for the bulk in Ref. 2. The slab calculations was checked by decoupling the breathing [setting $Q_\alpha(l_3\kappa, l_3'\kappa'; \bar{q}) = 0$] and using the same parameter values as Chen *et al.* used for MgO in Ref. 1. We were able to reproduce both the dispersion relations and surface-excess-frequency-distribution function given in Ref. 1.

III. RESULTS

In this section we present the results of our calculation in the form of the dispersion curves $\omega(\bar{q}p)$ and the frequency distribution functions $g_b(\omega)$, $g_s(\omega)$ and $f(\omega)$. The dispersion curves for the symmetric and the antisymmetric modes are shown separately. They are given for the high-symmetry lines $\bar{\Gamma}\bar{X}$, $\bar{X}\bar{M}$, and $\bar{M}\bar{\Gamma}$ in Figs. 2 and 3, and along the five special directions in Figs. 4–8. Fig. 1 shows the surface Brillouin zone (SBZ), the high-symmetry lines along the boundaries of the SBZ irreducible element, and the five special directions.

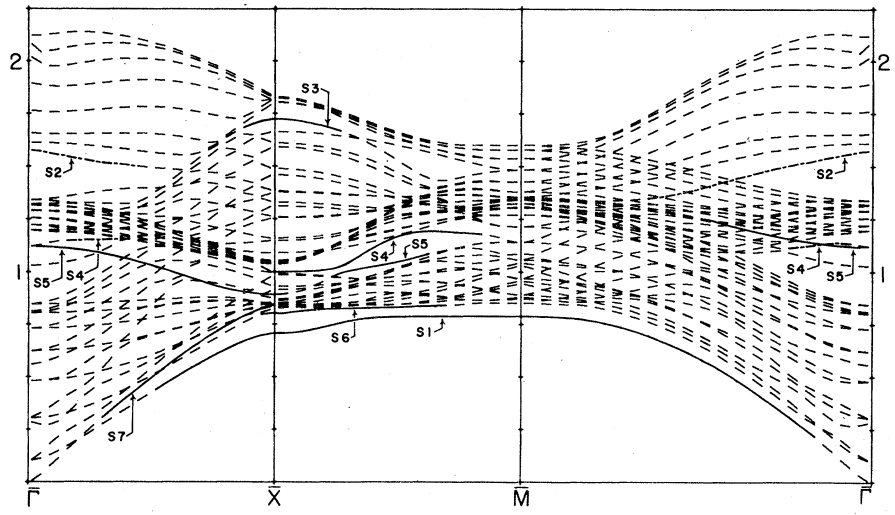

FIG. 2. Dispersion curves for the antisymmetric modes of a 15-layer unrelaxed MgO (001) slab for $\bar{q}$ along the high-symmetry lines $\bar{\Gamma}\bar{X}$, $\bar{X}\bar{M}$, and $\bar{M}\bar{\Gamma}$. The symbols Sn designating surface modes are explained in the text.

A. Dispersion curves

Most of the 90 dispersion curves of a 15-layer MgO slab fall into bulklike bands corresponding to the bulk LO, LA, TO, and TA curves. At the SBZ origin, $\bar{\Gamma}$, this identification is exact with the longitudinal modes having polarization vectors normal to the surfaces (longitudinal with respect to an imaginary third component of $\vec{q}$) and the transverse modes having polarization vectors parallel to the surfaces. Away from the origin along the high-symmetry lines $\bar{\Gamma}\bar{X}$ and $\bar{\Gamma}\bar{M}$ the normal modes are divided into two noninteracting polarization types, sagittal plane (SP) and shear horizontal (SH),[6] the sagittal plane being the plane normal to the surfaces containing the direction of $\bar{q}$. Thus along these high-symmetry lines there are six bulk subbands. They are the LO and LA subbands which are of the SP type, and the TO(SP), TO(SH), TA(SP), and TA(SH) subbands. Since modes of different polarization types are noninteracting the SP and SH subbands may cross or overlap and the individual curves are continuous. Where bands of the same polarization type cross or overlap, the individual curves are not continuous but rather are loci of hybridized curves. The same is true in the interior of the SBZ irreducible element where the dynamical matrix for each symmetry type, symmetric and antisymmetric, is not further reducible.

In addition to the bulklike modes there are seven surface modes of each symmetry. They occur in degenerate or almost degenerate pairs of opposite symmetry and are characterized by a rapid decrease in magnitude of core displacement away from the surfaces. These surface modes are

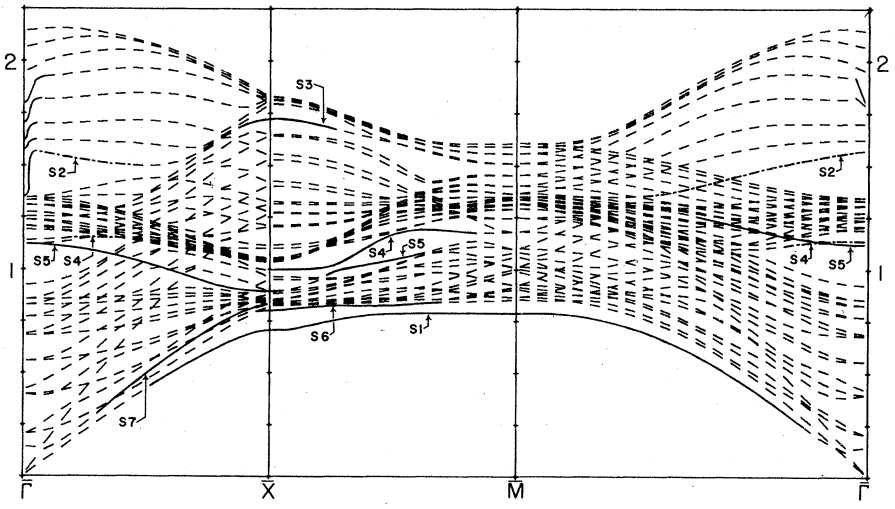

FIG. 3. Dispersion curves for the symmetric modes of a 15-layer MgO (001) slab for $\bar{q}$ along the high-symmetry lines.

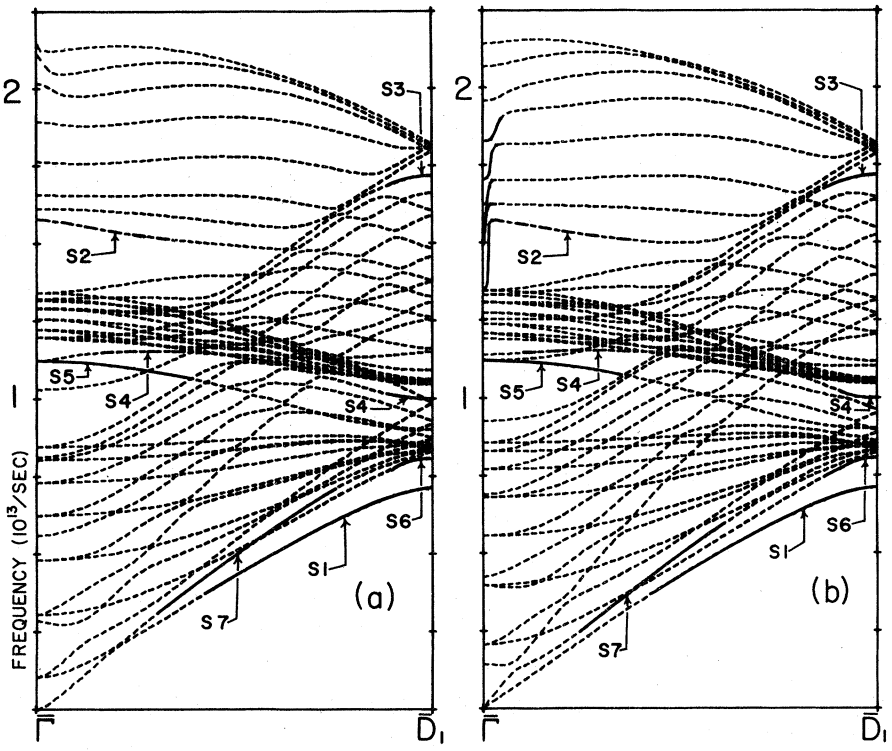

FIG. 4. Dispersion curves for a 15-layer unrelaxed MgO (001) slab along the special direction $\bar{\Gamma}\bar{D}_1$ in the interior of the SBZ, (a) antisymmetric modes and (b) symmetric modes. The symbols *Sn* designate surface modes as in Figs. 1 and 2.

labeled *Sn*, where *n* is a number between 1 and 7 assigned in the same manner as in Ref. 1. Surface modes are shown in the dispersion curve figures as solid lines, or as dot-dash lines for "pseudo surface modes" which have both bulklike and surface properties. Bulk modes are shown as dashed lines.

A surface mode may occur at the edge of or in gaps

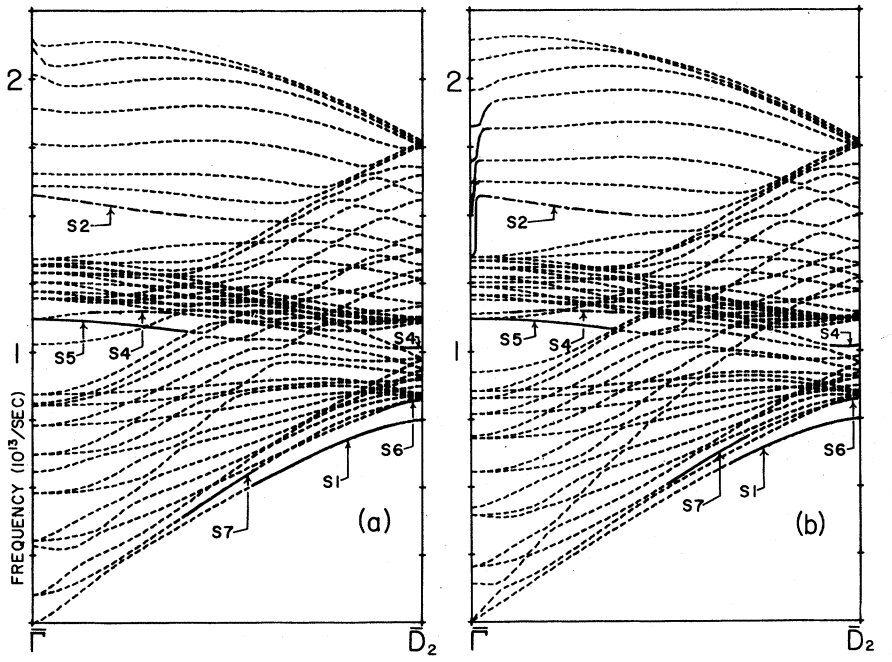

FIG. 5. Dispersion curves along the special direction $\bar{\Gamma}\bar{D}_2$, (a) antisymmetric modes and (b) symmetric modes.

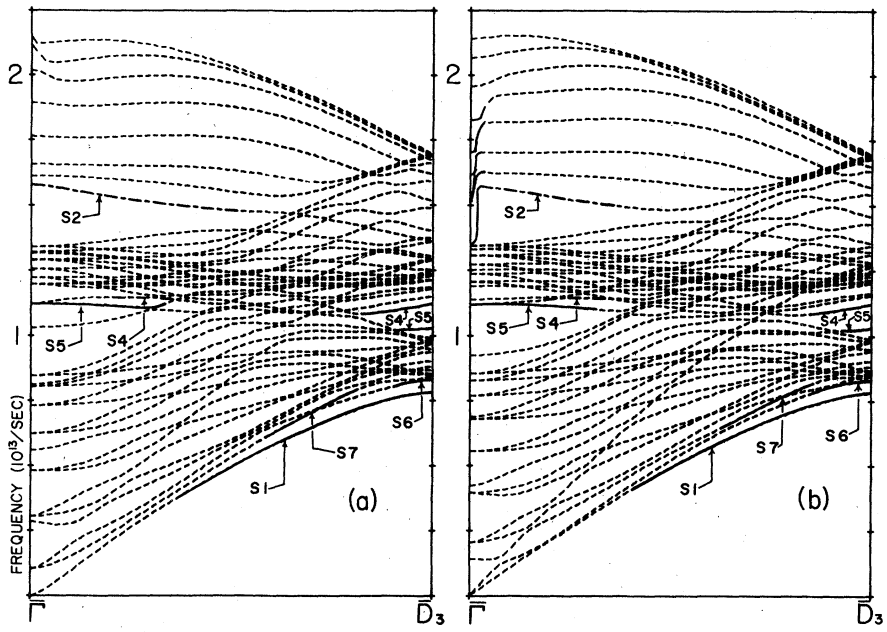

FIG. 6. Dispersion curves along the special directions $\bar{\Gamma}\bar{D}_3$, (a) antisymmetric modes and (b) symmetric modes.

between bulk subbands of the same polarization type, thus the structure of the bulk subbands plays an important role in determining the occurrence of surface modes. We now give a brief description of the behavior of the bulk subbands and the surface modes.

1. Bulk subbands

Along the direction $\bar{\Gamma}\bar{X}$, as $\bar{q}$ increases from the origin, the lower and upper edges of the TO(SP) and TA(SP) subbands lie above the corresponding edges of the TO(SH) and TA(SH) subbands. The LO subband moves up through the TO(SH) subband and overlaps the TO(SP) subband. As the angle between $\bar{q}$ and $\bar{\Gamma}\bar{X}$ increases the polarization characteristics of the transverse subbands are smoothly changed from SH to SP and vice versa so that along $\bar{\Gamma}\bar{M}$ the TO(SH) and TA(SH) band edges are above the corresponding TO(SP) and TA(SP) edges.

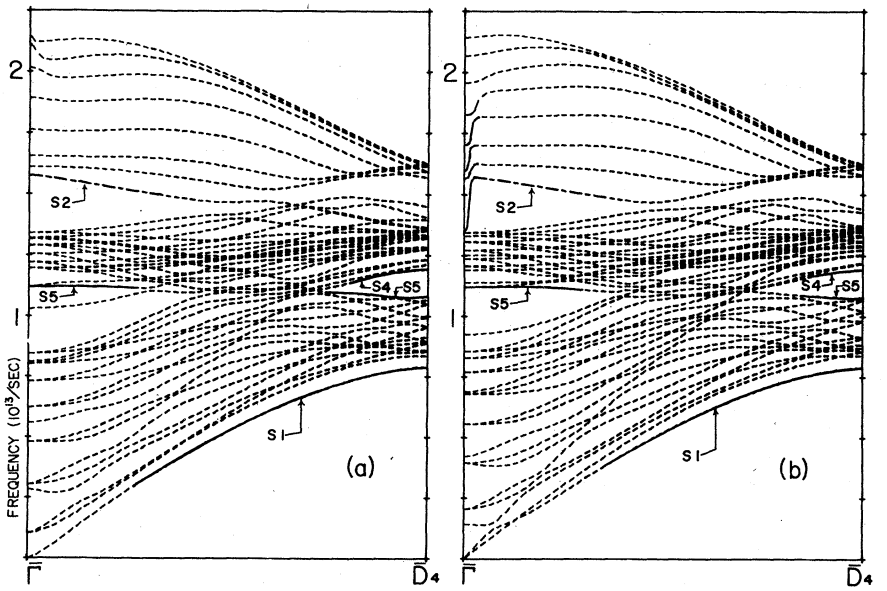

FIG. 7. Dispersion curves along the special direction $\bar{\Gamma}\bar{D}_4$, (a) antisymmetric modes and (b) symmetric modes.

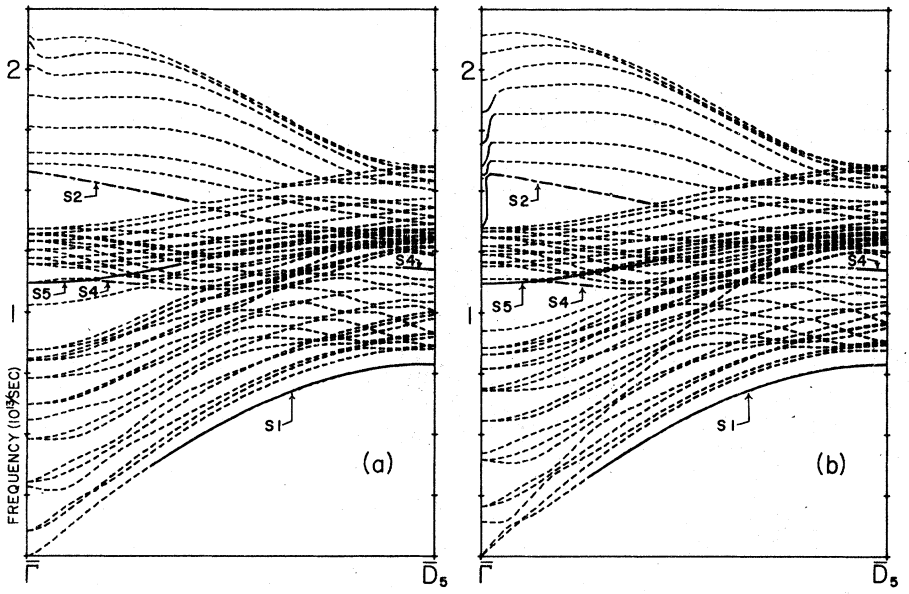

FIG. 8. Dispersion curves along the special direction $\bar{\Gamma}\bar{D}_5$, (a) antisymmetric modes and (b) symmetric modes.

2. *Macroscopic surface modes*

There are two types of surface modes which are derivable from continuum theory. These are the Fuchs-Kliewer (FK) modes from dielectric continuum theory and the Rayleigh modes from elastic continuum theory. The FK modes are not degenerate near the origin and are not shown in the dispersion curves. They are however evident near the origin as hybridizations involving the TO(SP) and LO modes. FK(−), the symmetric FK mode, shifts the frequency of each continuous curve up, starting at the bottom of the TO subband and continuing to near the top of the LO subband. FK(+) shifts the frequencies of the antisymmetric modes down near the top of the LO subband. According to Fuchs and Kliewer[8] the two should approach a common frequency a little below the LO bulk frequency but for a slab of only 15 layers the atomicity of the crystal becomes important before this happens and there is no degenerate surface mode pair corresponding to the FK modes.

The surface modes labeled $S1$ correspond to the Rayleigh modes. They are SH along $\bar{\Gamma}\bar{X}$, SP along $\bar{\Gamma}\bar{M}$, and lie below the bottom edge of the TA subband. The attentuation of the displacement away from the surface is inversely proportional to the wavelength, so for long wavelengths (small $\bar{q}$) they become bulklike and are not degenerate.

3. *Microscopic surface modes*

These other surface modes are not derivable from any continuum theory.

$S2$ and $S3$: These modes are found in the gaps between the LO and TO subbands. They are SP modes. $S2$ is unique to the breathing shell model for MgO, it did not occur in the non-breathing-model results of Ref. 1 although similar modes labeled $S2$ were found for some of the alkali halides. This pair follows the bottom edge of the LO subband from the origin until the top edge of TO subband approaches the LO subband. $S3$ occurs only in the gap between the LO and TO(SP) subbands near $\bar{X}$.

$S4$ and $S5$: the frequencies of both these pairs is the same at the origin. $S4$ is SP along $\bar{\Gamma}\bar{X}$ and SH along $\bar{\Gamma}\bar{M}$. It occurs as a locus of hybridized curves for some intermediate value of $\bar{q}$ away from the origin and reappears as a pair of continuous curves in the TO-TA gap, which exists along the SBZ boundary except near $\bar{M}$. $S5$ is SH along $\bar{\Gamma}\bar{X}$ and is a continuous curve all the way to $\bar{X}$. Along $\bar{\Gamma}\bar{M}$ it is SP and extends only about halfway. In the interior of the SBZ irreducible element it is a locus of hybridized curves extending out from the origin and reappears in the TO-TA gap at the boundary. In the nonbreathing model of Ref. 1 $S4$ and $S5$ cross as $\bar{q}$ moves along the boundary line $\bar{X}\bar{M}$, but in our result $S5$ remains below $S4$. The fourfold degeneracy of $S4$ and $S5$ at the origin suggests that they might be subject to direct experimental verification; however, no such verification has been made.

$S6$ and $S7$: These are acoustic surface modes found at or near the bottom edge of the TA subband. $S6$ occurs at the bottom edge of the TA subband only near the SBZ boundary. It is SH at $\bar{X}$ and approaches being SP before disappearing near

$\bar{M}$. $S7$ is SH along $\bar{\Gamma}\bar{X}$ and is a continuous curve except near the origin, following the bottom edge of the TA(SH) band all the way to $\bar{X}$. In the interior of the SBZ irreducible element it occurs as a locus of hybridized curves for some intermediate values of $\bar{q}$ and disappears entirely as the two TA subbands exchange polarization characteristics. $S7$ does not occur along $\bar{\Gamma}\bar{M}$.

These results, except for the occurrence of $S2$, resemble very closely the results for the nonbreathing-shell model, and we refer to Ref. 1 for a more complete description of the surface-mode characteristics.

B. Frequency distribution functions

The bulk frequency distribution function for our model is shown in Fig. 9 and may be compared to the distribution function shown for model D of Ref. 2 since the parameters are almost the same. The slab distribution function, $g_s(\omega)$, is shown in Fig. 10 and the surface excess distribution function, $f(\omega)$, in Fig. 11. Also in Fig. 11 we show the experimental surface-excess-distribution function of Rieder[5] as a dashed line, scaled in arbitrary units to fit in the $f(\omega)$ frame. The distribution functions were all obtained initially as 450 bin histograms and then smoothed so that each bin $g(n)$ in the smoothed function is a weighted average of several bins $g(n \pm m)$, $m = 0, 1, 2, \ldots$. The weighting function is the normal distribution function $e^{-m^2/2\sigma^2}$, where σ is adjustable to control the range over which the functions are smoothed. For the bulk and slab $2\sigma \simeq 0.033 \times 10^{13}$ sec^{-1} and for the surface excess $2\sigma \simeq 0.048 \times 10^{13}$ sec^{-1}. The bulk

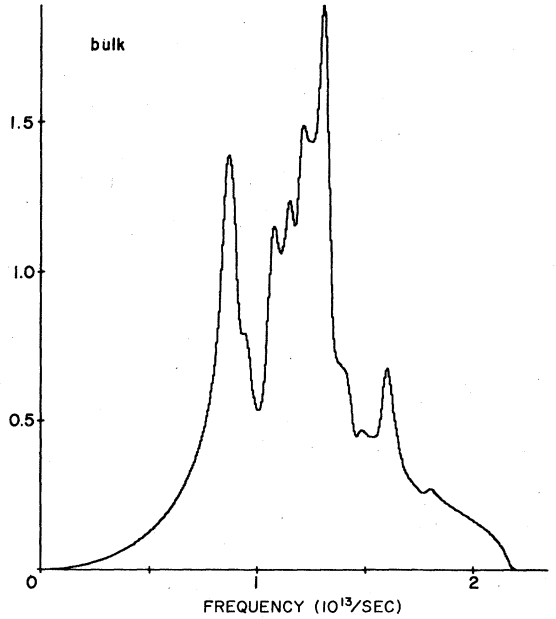

FIG. 9. Bulk (infinite crystal) frequency distribution for MgO from the breathing-shell model discussed in the text, smoothed over a frequency interval of 0.033 $\times 10^{13}$ sec^{-1}.

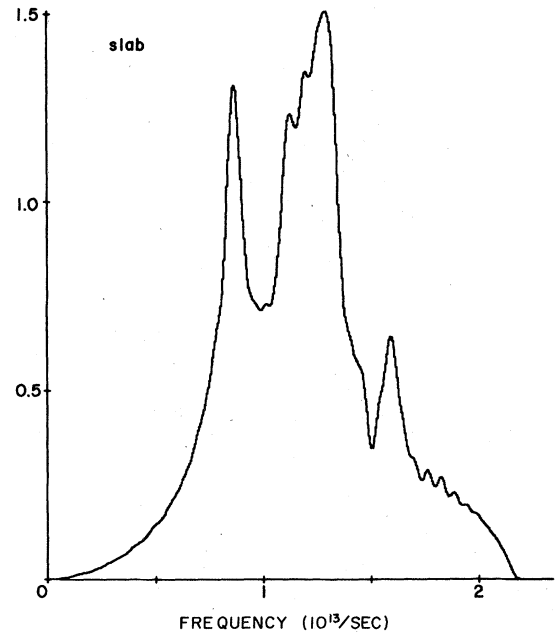

FIG. 10. Frequency distribution function for a 15-layer unrelaxed MgO (001) slab from the breathing-shell model discussed in the text, smoothed over a frequency interval of 0.033 $\times 10^{13}$ sec^{-1}.

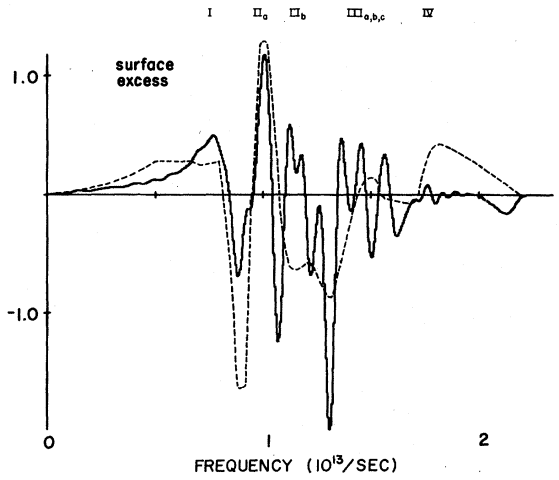

FIG. 11. Surface-excess frequency distribution function for a 15-layer unrelaxed MgO (001) slab from the breathing-shell model discussed in the text, smoothed over a frequency interval of 0.048 $\times 10^{13}$ sec^{-1}. The dashed curve is the experimental result of Rieder.[5]

and slab frequency distribution functions are normalized to unity.

The maxima and minima in the surface-excess distribution function are due to the flat portions of the surface-mode dispersion curves and the depletion of bulk subbands associated with the formation of surface modes. The surface-excess function of our model shows more structure than is seen in the experimental function, particularly at frequencies above 10^{13} sec^{-1}, but the experimental resolution does decrease with increasing frequency. The main features are in reasonable agreement except for the wide peak in the experimental result near the maximum frequency.

The peaks of the experimental surface-excess frequency-distribution function are labeled in Fig. 11 by Roman numerals, and the subscripts a, b, c refer to corresponding individual peaks in the model function. The peaks may be attributed to the surface modes as follows: I, due to $S1, S6$, and $S7$; II_a, due to $S4$ near $\bar{X}$ and $S5$ along $\bar{X}\bar{M}$; II_b, due to $S4$ and $S5$ near $\bar{\Gamma}$ and $S4$ along $\bar{X}\bar{M}$ away from $\bar{X}$; $\mathrm{III}_{a,b,c}$, due to the lower reaches of $S2$ along $\bar{\Gamma}\bar{M}$, along $\bar{\Gamma}\bar{X}$, and to $S2$ near $\bar{\Gamma}$, respectively; and IV, due to $S3$. The minimum in the model distribution function above 2×10^{13} sec^{-1} is attributed to FK(+) shifting the antisymmetric LO modes down in frequency.

C. Summary

The breathing-shell model has been used because it gives significantly better agreement with experimental results for the bulk lattice dynamics, and because previous calculations have shown that the breathing mode has a nonnegligible effect on surface relaxation. The principle differences between the breathing and the normal-shell-model dispersion curves are the occurrence of surface mode $S2$ and a shift in frequency of surface modes $S4$ and $S5$ at the SBZ boundary. There are corresponding differences, i.e., peaks II_b and $\mathrm{III}_{a,b,c}$, in the surface-excess frequency distribution functions. It is hoped that the results reported here will be of interest to others working in the same area and will be a basis for comparison with future more realistic model calculations including surface relaxation.

ACKNOWLEDGMENTS

We thank G. P. Alldredge, F. W. de Wette, and R. Fuchs for useful and instructive conversations. Partial support for this work was provided by University of Kansas General Research Allocations Nos. 3054-x038 and 3087-x0038. One of us (R.N.B.) thanks the University of Kansas Graduate School for a Dissertation Fellowship.

APPENDIX

The matrix elements coupling the breathing mode to the core and shell displacements are as follows:

(a) If $|l_3 - l_3'| \geq 2$, $Q_\alpha(l_3\kappa, l_3'\kappa'; \bar{q}) = 0$.

(b) $Q_\alpha(l_3 1, l_3' 1; \bar{q})$ does not appear in the equations of motion since the breathing of the Mg^{2+} ions is neglected.

(c) If $|l_3 - l_3'| = 1$,

$$Q_3(l_3 2, l_3' 2; \bar{q}) = [(l_3 - l_3')/(|l_3 - l_3'|)](e^2/2V)\sqrt{2}\,A' \times [\cos(q_1 r_0) + \cos(q_2 r_0)],$$

$$Q_1(l_3 2, l_3' 2; \bar{q}) = (e^2/2V)\sqrt{2}\,A' i \sin(q_1 r_0),$$

$$Q_2(l_3 2, l_3' 2; \bar{q}) = (e^2/2V)\sqrt{2}\,A' i \sin(q_2 r_0),$$

$$Q_3(l_3 1, l_3' 2; \bar{q}) = [(l_3 - l_3')/|l_3 - l_3'|](e^2/2V)A,$$

$$Q_1(l_3 1, l_3' 2; \bar{q}) = Q_2(l_3 1, l_3' 2; \bar{q}) = 0.$$

(d) If $|l_3 - l_3'| = 0$,

$$Q_3(l_3 2, l_3 2; \bar{q}) = -(e^2/2V)(A + 2\sqrt{2}\,A')[\delta(l_3) - \delta(l_3 - N)],$$

$$Q_1(l_3 2, l_3 2; \bar{q}) = (e^2/2V)2\sqrt{2}\,A' i \sin(q_1 r_0)\cos(q_2 r_0),$$

$$Q_2(l_3 2, l_3 2; \bar{q}) = (e^2/2V)2\sqrt{2}\,A' i \sin(q_2 r_0)\cos(q_1 r_0),$$

$$Q_3(l_3 1, l_3 2; \bar{q}) = 0,$$

$$Q_1(l_3 1, l_3 2; \bar{q}) = (e^2/2V)2A i \sin(q_1 r_0),$$

$$Q_2(l_3 1, l_3 2; \bar{q}) = (e^2/2V)2A i \sin(q_2 r_0),$$

where $l_3 = 1, \ldots, N$; A, B, A', and B' are the short-range interaction parameters as defined in Ref. 2; e is the proton charge; and $V = 2r_0^3$ is the simple cell volume, r_0 is the nearest-neighbor distance.

The breathing-breathing matrix elements are as follows:

(a) If $|l_3 - l_3'| \geq 2$, $H(l_3\kappa, l_3'\kappa'; \bar{q}) = 0$.

(b) $H(l_3\kappa, l_3' 1; \bar{q})$ does not appear in the equations of motion since the breathing of the Mg^{2+} ion is neglected.

(c) If $|l_3 - l_3'| = 1$,

$$H(l_3 2, l_3' 2; \bar{q}) = (e^2/2V)2A'[\cos(q_1 r_0) + \cos(q_2 r_0)].$$

(d) If $|l_3 - l_3'| = 0$,

$$H(l_3 2, l_3 2; \bar{q}) = (e^2/2V)\{4A'\cos(q_1 r_0)\cos(q_2 r_0) + 6A + 12A' - (A + 4A') \times [\delta(l_3) + \delta(l_3 - N)]\}.$$

[1]T. S. Chen, F. W. de Wette, and G. P. Alldredge, Phys. Rev. B 15, 1167 (1977).
[2]M. J. L. Sangster, G. Peckham, and D. H. Saunderson, J. Phys. C 3, 1026 (1970).
[3]M. J. L. Sangster, J. Phys. Chem. Solids 35, 195 (1974).
[4]R. N. Barnett and R. Bass, J. Chem. Phys. 67, 4620 (1977).
[5]K. H. Rieder, Surf. Sci. 26, 637 (1971).
[6]R. E. Allen, G. P. Alldredge, and F. W. de Wette, Phys. Rev. B 4, 1648 (1971).
[7]A. Bansil, Solid State Commun. 16, 885 (1975).
[8]R. Fuchs and K. L. Kliewer, Phys. Rev. 140, A 1076 (1965).